Applied Catalysis B: Environmental 144 (2014) 1–11

Contents lists available at ScienceDirect

Applied Catalysis B: Environmental

journal homepage: www.elsevier.com/locate/apcatb

# Surface fluorination of single-phase $TiO_2$ by thermal shock method for enhanced UV and visible light induced photocatalytic activity

Tien Khoa Le[a,b], Delphine Flahaut[b], Hervé Martinez[b], Thierry Pigot[b], Huu Khanh Hung Nguyen[a], Thi Kieu Xuan Huynh[a,*]

[a] University of Science – VNU Ho Chi Minh City, 227 Nguyen Van Cu Street, Ho Chi Minh City, Viet Nam
[b] IPREM/ECP (UMR 5254), University of Pau, Hélioparc, 2 av. Pierre Angot, 64053 Pau cedex 9, France

ARTICLE INFO

*Article history:*
Received 16 April 2013
Received in revised form 6 June 2013
Accepted 20 June 2013
Available online 1 July 2013

*Keywords:*
Fluorination
Monophasic $TiO_2$
Thermal shock
Adsorption behaviour
Photocatalytic activity

ABSTRACT

Fluorinated $TiO_2$ was prepared from anatase and rutile monophasic $TiO_2$ nanopowders by thermal shock method at different temperatures (400–950 °C), then characterized by XRD, SEM, XPS in order to elucidate the influences of thermal shock fluorination on the crystallite structure, morphologies and surface structure of $TiO_2$ in different phases. Their photocatalytic activities were evaluated via the degradation of methylene blue. According to the results, the fluorination below 600 °C did not change the crystallite structure or the particle size. However, the surface hydroxyl groups content is increased with the creation of fluoride ions and oxygen/titanium vacancies on the surface of anatase/rutile $TiO_2$ which are all involved in the improvement of the photocatalytic activity. The $TiO_2$ anatase fluorinated at 500 °C showed the best photocatalytic behaviour under UV light whereas the $TiO_2$ rutile fluorinated at 500 °C is the best photocatalyst under visible light. At higher thermal shock temperatures, the photocatalytic activity decreased, which was assigned to the decrease of the surface hydroxyl groups and vacancies content and the formation of the $K_2Ti_6O_{13}$ phase.



## 1. Introduction

Over the past decades, heterogeneous semiconductor photocatalysts based on $TiO_2$ nanoparticles have been intensively studied in various fields, especially for the degradation of environmental pollutants [1]. Among various $TiO_2$ photocatalysts, $TiO_2$ P25, a mixture of anatase and rutile with a primary particle size of 20–30 nm, has been currently studied and used as the catalyst for environment treatment because it is so far the best commercial photocatalyst [2,3]. However, for practical applications, the photocatalytic activity of $TiO_2$ still needs to be further improved. Some studies have performed the F doping in the lattice of $TiO_2$ by the sol–gel method [4] or spray pyrolysis [5] in order to improve the photocatalytic activity. Recently, surface fluorination of $TiO_2$ by a simple ligand exchange [2,6,7] or solvothermally treatment [8] has also been found to be a most effective and simple method to increase the $TiO_2$ induced photocatalytic degradation of diverse dyes, such as methylene blue [6], rhodamine B [7], methyl orange [8]. In previous work [9], we described a new and efficient approach for the preparation of fluorinated $TiO_2$ P25 powders by thermal shock (TS) method at several temperatures from 400 to 950 °C. This method has successfully fluorinated the surface of $TiO_2$ P25, created oxygen vacancies and increased the surface hydroxyl groups content. This contributed to an improvement of the activity of this oxide under visible irradiation. Nevertheless, as far as we know, the photocatalytic behaviour of a biphasic anatase and rutile like $TiO_2$ P25 is quite different from anatase or rutile single-phase $TiO_2$ powder [10–13]. More especially, the optical and photocatalytic properties of $TiO_2$ anatase are also different from $TiO_2$ rutile. Thus the fluorination of monophasic $TiO_2$ nanopowder in different phases by thermal shock process might be interesting and give promising results.

Therefore, in this study, we have performed the fluorination of anatase and rutile monophasic $TiO_2$ nanopowders by thermal shock (TS) method in order to investigate the influence of the fluorination process on their bulk structure, morphology, surface composition and optical properties. The photocatalytic activity of anatase fluorinated $TiO_2$ was compared with rutile fluorinated $TiO_2$ via the degradation of methylene blue (MB) as the target organic pollutant. The origin of UV and visible light response as well as the mechanism of photocatalytic MB degradation on the fluorinated monophasic $TiO_2$ powders was also discussed in detail in this paper.

## 2. Experimental

### 2.1. Sample preparation

Monophasic anatase and rutile $TiO_2$ nanoparticles were purchased from Sigma–Aldrich. KF (99%, extra pure grade) and

* Corresponding author. Tel.: +84 8 38 30 21 46; fax: +84 8 38 35 00 96.
*E-mail address:* htkxuan@hcmus.edu.vn (T.K.X. Huynh).

0926-3373/$ – see front matter © 2013 Elsevier B.V. All rights reserved.
http://dx.doi.org/10.1016/j.apcatb.2013.06.027

methylene blue (MB) (analytical grade) from Merck. All chemicals used in this study were of analytical grade and were used as received without further purification. Distilled water was used in all the experiments.

Firstly, monophasic (anatase or rutile) $TiO_2$ nanoparticles were suspended in 10 mL of a KF solution (0.625 mol $L^{-1}$) with the molar ratio of fluorine to titanium of 1:1. The obtained white suspension was dried at 150 °C for 3 h. The dried powders were rapidly put into a furnace for a thermal shock (TS) of 5 min at several temperatures: 400, 500, 600, 700, 800 and 950 °C. Then, the samples were washed with 100 mL of distilled water through a membrane filtration for 5 times to remove the remained KF on the surface of samples and dried again at 150 °C for 1 h. This thermal shock method is identical to that used in our previous study [9]. In the following manuscript, the fluorinated samples from anatase and rutile were labelled as AFTO-X and RFTO-X, respectively (with X the temperature of thermal shock process).

### 2.2. Characterization

The X-ray diffraction (XRD) measurements, which were used to characterize the crystalline structure and phase composition of fluorinated $TiO_2$ samples, were carried out by an SIEMENS D5000 X-ray diffractometer using Cu Kα radiation (λ = 1.5406 Å). The accelerating voltage and the applied current were 40 kV and 25 mA, respectively.

The morphology of fluorinated samples was observed by a scanning electron microscopy (SEM) using a Auger Microprobe JAMP 9500F which operates at the probe current of $10^{-10}$ Å and 30 keV and a working distance (source/sample) of about 20 mm.

The X-ray photoelectron spectra (XPS) was made in a Thermo K-alpha system with a hemispherical analyzer and a microfocussed (analysis area was ca. 200 $\mu m^2$) monochromatized radiation Al Kα line (1486.6 eV) operating at 75 W under a residual pressure of $1 \times 10^{-7}$ mbar in order to characterize the surface atomic composition and chemical environment of elements at surface of all samples. The spectrometer pass energy was set to 200 eV for survey spectrum and to 20 eV for core peak records. Surface charging was minimized using a neutralizer gun which sprays the low energy electrons and $Ar^+$ ions over the sample surface. All the binding energies were referenced to the C 1s peak at 285.0 eV originating from the surface carbon contamination. The treatment of core peaks was carried out using a nonlinear Shirley-type background [14]. A weighted least-squares fitting method using 70% Gaussian, 30% Lorentzian line shapes was applied to optimize the peak positions and areas. The quantification of surface composition was based on Scofield's relative sensitivity factors [15].

### 2.3. Adsorption of methylene blue

Prior to the photocatalytic experiments, the MB adsorption on the surface of catalysts were carried out to study the influence of surface fluorination on the interaction of catalyst surface with the dye MB compound. 0.125 g naked $TiO_2$ sample or fluorinated samples were respectively added to 250 mL of a $10^{-5}$ mol $L^{-1}$ MB aqueous solution. Then the received suspension was magnetically stirred in the dark condition during 30 min. Finally, the sampling and the filtration were performed. The MB concentration of filtered solutions was determined by measuring their absorbance at 660 nm with a SP-300 Optima spectrophotometer. We kept stirring the suspension in the dark for the next 30 min and checked again its concentration in order to ensure that the adsorption/desorption equilibrium between the $TiO_2$ surface and the MB was obtained.

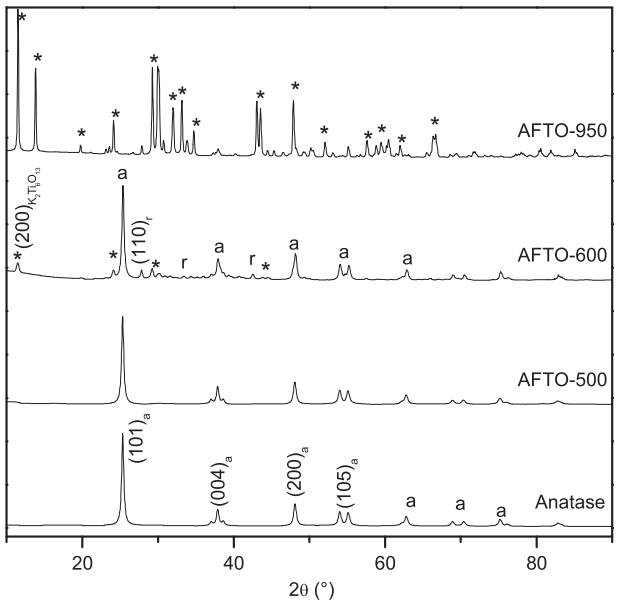


**Fig. 1.** XRD patterns of fluorinated samples from anatase: anatase, AFTO-500, AFTO-600 and AFTO-950 (a, r, * represent the anatase, rutile and $K_2Ti_6O_{13}$-type phases, respectively).

### 2.4. Photocatalytic degradation of dye

The photocatalytic activities of bare and fluorinated $TiO_2$ samples were evaluated through the degradation of MB. The tests were performed in a reactor which consists of a glass beaker containing 250 mL of reaction solution with catalyst, cooled by continuous water flow and stirred continuously by magnetic agitator. The reaction solution was irradiated by an 8-W UV light lamp (350 nm) or an 8-W visible light lamp (420 nm) placed about 10 cm above the solution surface. The temperature of system was maintained at 30 °C.

The initial concentrations of catalysts and aqueous MB solution were identical to those used in the adsorption study (0.5 g $L^{-1}$ for catalysts and $10^{-5}$ mol $L^{-1}$ for MB solution). The suspensions were dispersed in an ultrasonic bath for 15 min to disperse the large aggregates before putting into the reactor. The pH of suspensions was fixed at 7 and the reaction temperature was maintained at 30 °C during the experiments. Prior to irradiation, the suspension was magnetically stirred in the dark for 30 min to ensure the adsorption/desorption equilibrium. During the illumination, 10 mL of suspension was sampled every 30 min, centrifuged and analyzed by SP-300 Optima spectrophotometer.

## 3. Results and discussion

### 3.1. Phase structures

XRD was used to follow the effects of fluorination on the crystallite structures and phase compositions of single-phase anatase and rutile $TiO_2$ nanoparticles. Figs. 1 and 2 show the XRD patterns of the bare and fluorinated $TiO_2$ in the anatase and rutile forms. The Rietveld refinement was carried out using the Fullprof 2009 structure refinement software [16]. The cell parameters and percentage of different crystallographic phases are summarized in Table 1.

The naked anatase $TiO_2$ sample (Fig. 1) exhibits a pure anatase phase (space group $I4_1/amd$, JCPDS No. 21-1272), identified by the XRD peaks at 25.25° ((1 0 1) line), 37.85° ((0 0 4) line), 48.11° ((2 0 0) line) and 54.11° ((1 0 5) line). No additional phase and no evolution of the cell parameters have been detected in the XRD patterns of fluorinated samples prepared up to 500 °C. However, two

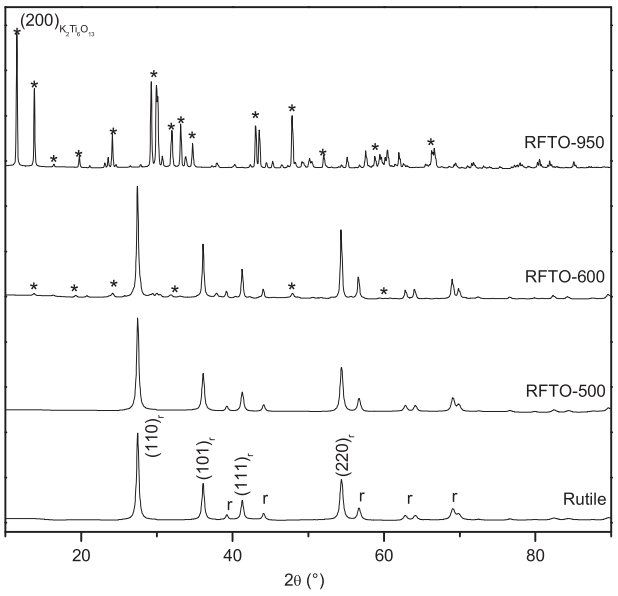


**Fig. 2.** XRD patterns of fluorinated samples from rutile: rutile, RFTO-500, RFTO-600 and RFTO-950 (a, r, * represent the anatase, rutile and $K_2Ti_6O_{13}$-type phases, respectively).

additional crystallographic phases were identified for the AFTO-600 sample. The XRD peaks at 27.44° ((1 1 0) line), 36.06° ((1 0 1) line), 41.23° ((1 1 1) line) are characteristic of the $TiO_2$ rutile phase (space group $P4_2/mnm$, JCPDS No. 21-1276) which was expected since the anatase/rutile transition occurs at around 700 °C [17]. As reported in our previous paper [9], the fluorination method used to conduct to the formation of the $K_2Ti_6O_{13}$–type phase (space group C2/m, JCPDS No. 73-1398) was clearly identified by the XRD peaks located at 11.45° ((2 0 0) line), 24.10° ((1 1 0) line), 29.20° ((3 1 0) line) and 42.92° ((−4 0 4) line). The contribution of this phase to the XRD pattern is increasing with the temperature while those of anatase and rutile phases are dropping.

As reported for the anatase samples, the XRD patterns (Fig. 2) of the rutile phase samples are not modify by the fluorination up to 500 °C. As expected, we also observe the appearance of $K_2Ti_6O_{13}$ phase beside the rutile one above 600 °C with a decline of the rutile phase content.

### 3.2. Morphology

As observed from the SEM images (Figs. 3 and 4a), the particles of naked anatase and rutile $TiO_2$ samples are nearly spherical in shape with a homogeneous size distribution of 20–50 nm and 30–70 nm for anatase and rutile, respectively. The shape and size of particles remained unchanged for a fluorination by TS at 500 °C (Figs. 3 and 4b). Nevertheless, we can observe the formation of small

**Table 1**
Phase composition and cell parameters of fluorinated samples from anatase and rutile phases.

| Sample | Fraction (%) ($R_{Bragg}/R_f$) | | |
|---|---|---|---|
| | Anatase | Rutile | $K_2Ti_6O_{13}$ |
| Anatase | 100 ± 2 (7.56/8.27) | | |
| AFTO-500 | 100 ± 2 (14.2/13.5) | | |
| AFTO-600 | 80 ± 2 (18.0/14.2) | 5.8 ± 0.8 (34.2/27.4) | 14.1 ± 0.7 (48.8/45.0) |
| AFTO-950 | | | 100 ± 2 (19.7/22.6) |
| Rutile | | 100 ± 2 (10.8/17.2) | |
| RFTO-500 | | 100 ± 2 (9.5/11.0) | |
| RFTO-600 | | 91 ± 2 (17.9/14.4) | 8.9 ± 0.5 (48.1/31.0) |
| RTO-950 | | | 100 ± 2 (20.3/27.4) |

**Table 2**
High resolution XPS data of fluorinated anatase $TiO_2$ samples: binding energies (eV), FWHM (eV) in parentheses and atomic percentages (%).

| | Anatase | | AFTO-400 | | AFTO-500 | | AFTO-600 | | AFTO-700 | | AFTO-800 | | AFTO-950 | |
|---|---|---|---|---|---|---|---|---|---|---|---|---|---|---|
| | $E_B$ (FWHM) eV | % | $E_B$ (eV) | % | $E_B$ (eV) | % | $E_B$ (eV) | % | $E_B$ (eV) | % | $E_B$ (eV) | % | $E_B$ (eV) | % |
| C 1s | 285.0 (1.5) | 11.2 | 285 (1.4) | 10.8 | 285.0 (1.5) | 8.5 | 285.0 (1.5) | 11.1 | 285.0 (1.4) | 8.3 | 285.0 (1.5) | 8.3 | 285.0 (1.5) | 9.7 |
| | 286.6 (1.5) | 1.9 | 286.5 (1.5) | 1.3 | 286.6 (1.4) | 0.7 | 286.6 (1.4) | 1.4 | 286.1 (1.6) | 0.7 | 286.4 (1.6) | 1.2 | 286.5 (1.5) | 1.9 |
| | 289.1 (1.5) | 1.2 | 289.1 (1.6) | 1.0 | 289.3 (1.4) | 0.4 | 289.3 (1.3) | 0.6 | 289.4 (0.7) | 0.2 | 289.6 (1.4) | 0.6 | 289.4 (1.5) | 0.3 |
| Ti $2p_{3/2-1/2}$ | 459.0–464.7 (1.0–1.9) | 26.6 | 458.8–464.6 (1.0–1.9) | 25.3 | 458.9–464.6 (1.0–1.9) | 26.1 | 459.0–464.8 (1.1–2.0) | 22.61 | 459.1–464.8 (1.2–2.0) | 23.9 | 459.2–464.9 (1.2–2.1) | 23;7 | 459.0–464.8 (1.3–2.1) | 21.2 |
| Satellites | 471.8–478.2 | | 471.7–478.1 | | 471.7–478.4 | | 471.8–478.2 | | 471.9–478.3 | | 472.1–478.2 | | 471.7–478.2 | |
| O 1s I | 530.3 (1.1) | 53.1 | 530.1 (1.1) | 49.2 | 530.1 (1.1) | 50.8 | 530.4 (1.2) | 43.8 | 530.5 (1.2) | 46.5 | 530.7 (1.3) | 47.2 | 530.5 (1.3) | 42.2 |
| O 1s II | 531.6 (1.6) | 6.0 | 531.4 (1.6) | 7.0 | 531.5 (1.6) | 7.3 | 531.6 (1.6) | 8.5 | 531.6 (1.6) | 6.8 | 531.7 (1.6) | 5.7 | 531.6 (1.6) | 6.2 |
| O 1s III | | | 532.7 (1.6) | 1.7 | 532.9 (1.6) | 0.8 | 532.9 (1.6) | 2.8 | 532.9 (1.6) | 1.1 | 532.9 (1.6) | 2.0 | 532.9 (1.6) | 5.4 |
| F 1s I | | | 684.5 (1.6) | 2.4 | 684.4 (1.6) | 3.3 | 684.7 (1.6) | 4.6 | 684.7 (1.6) | 5.8 | 685.0 (1.6) | 4.0 | 684.8 (1.6) | 4.7 |
| F 1s II | | | 686.4 (1.6) | 0.3 | 686.5 (1.6) | 0.2 | 686.7 (1.6) | 0.4 | 686.3 (1.6) | 0.4 | 686.5– | | | |
| 689.6 (1.6) | 0.8 | | | | | | | | | | | | 686.7–688.0–689.7 (1.6) | 1.7 |
| K $2p_{3/2-1/2}$ I | | | 292.9–295.6 (1.1–1.1) | 0.5 | 292.9–295.6 (1.0–1.1) | 1.1 | 292.7–295.5 (1.1–1.2) | 2.2 | 292.8–295.6 (1.1–1.2) | 4.5 | 292.8–295.6 (1.0–1.1) | 5.61 | 292.7–295.4 (1.1–1.1) | 5.2 |
| K $2p_{3/2-1/2}$ II | | | 293.7–296.4 (1.1–1.1) | 0.5 | 293.6–296.3 (1.1–1.1) | 1.0 | 293.5–296.2 (1.2–1.2) | 2.0 | 293.8–296.5 (1.1–1.3) | 1.9 | 293.8–296.5 (1.1–1.1) | 1.15 | 293.7–296.4 (1.2–1.2) | 1.4 |

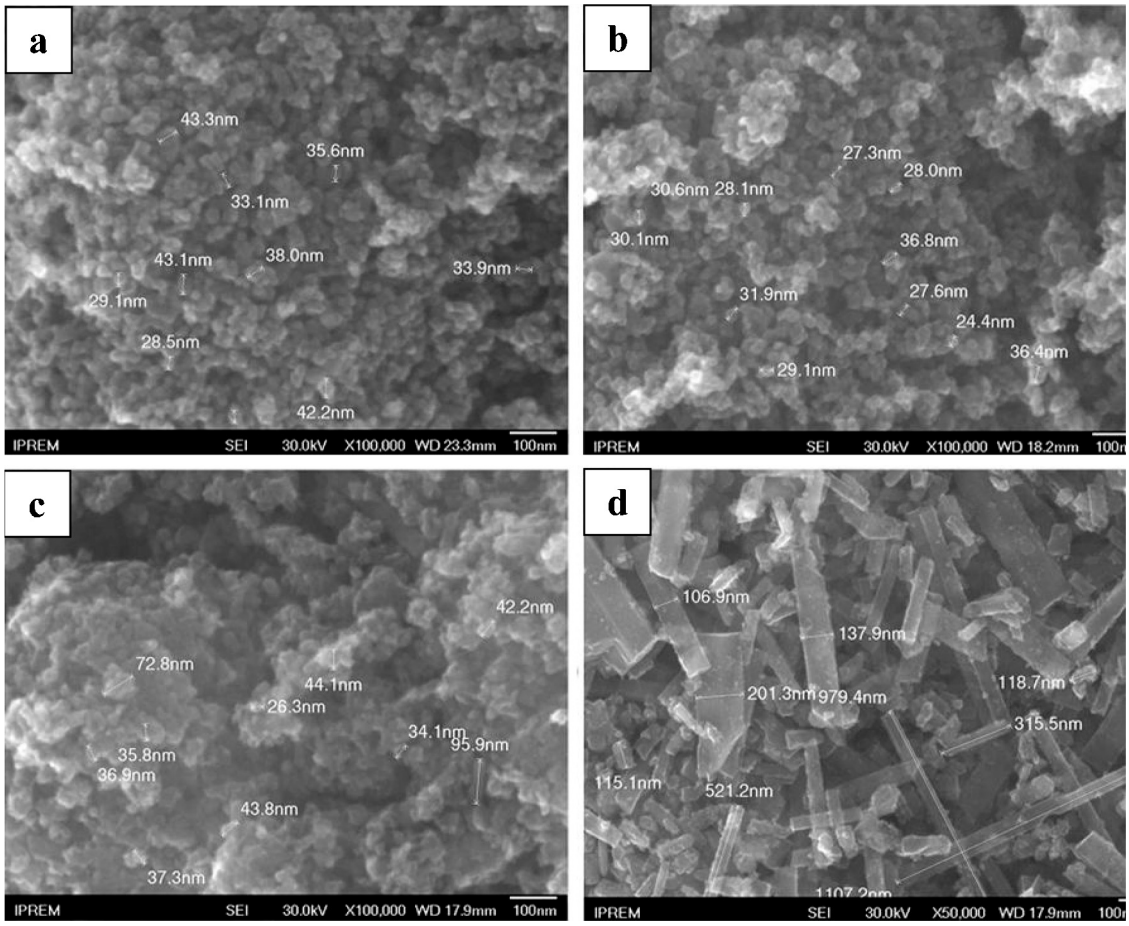


**Fig. 3.** SEM micrographs of (a) anatase, (b) AFTO-500, (c) AFTO-600 and (d) AFTO-950.

rod-like particles (70–100 nm in length) among $TiO_2$ spherical particles (Figs 3 and 4c) for a fluorination above 600 °C, which is in fairly good agreement with the appearance of $K_2Ti_6O_{13}$ phase from XRD patterns of AFTO-600 and RFTO-600 samples. Up to 950 °C, these rod-like $K_2Ti_6O_{13}$ particles become dominant and can reach a length around 900–1000 nm (Figs. 3 and 4d).

### 3.3. XPS analysis

The surface fluorination and the relative concentration and chemical environment of F, O, Ti and C atoms on the surface of the catalysts were followed by XPS. The results are reported in Tables 2 and 3. The C 1s core peaks is due to the surface contamination carbon and can be decomposed into three peaks: the main peak at 285.0 eV associated with C—C or C—H bonds, the peak at 286.6 eV with C—O bonds and the peak at 289.1 eV with O=C—O bonds. As shown in Fig. 5, due to spin–orbit coupling, the Ti 2p core peaks of all the samples exhibit two main Ti 2p components at around 459.0 eV (Ti $2p_{3/2}$) and 464.7 eV (Ti $2p_{1/2}$), followed by charge-transfer satellite peaks at 13 eV above the $2p_{3/2}$ and $2p_{1/2}$ peaks positions. The binding energy (B.E.) is representative of the $Ti^{4+}$ ions in $TiO_2$ [18,19]. The evolution of the Ti 2p spectra also indicates that the fluorination does not modify the oxidation state and the chemical environment of titanium atoms at the surface of $TiO_2$. Fig. 6a and b exhibits the F 1s spectra of, respectively, the anatase and rutile fluorinated powders. For the anatase and rutile single-phase $TiO_2$ fluorinated up to 700 °C, the F 1s core peaks consistd of a main peak located at 684.5 eV ($F_I$) assigned to the fluoride ions chemisorbed on the surface [8,20] and a minor peak at 686.7 eV ($F_{II}$) which corresponds to fluorine atoms in oxygenated environment of solid solution $TiO_{2-x}F_x$ due to the substitution of F ions for O ions in the $TiO_2$ lattice [4,5]. This indicates that our simple method at low TS temperature could insert the fluorine atoms in the $TiO_2$ surface structure. The calculation of $F_I$/Ti and $F_{II}$/Ti atomic ratios put in evidence the increase of the fluor amount on the surface ($F_I$/Ti = 0.09–0.25 for AFTO and $F_I$/Ti = 0.10–0.18 for RFTO) and a slight increase of F amount in the lattice of $TiO_2$ ($F_{II}$/Ti = 0.01–0.02 for AFTO and RFTO) with TS temperatures (Table 4). Above 700 °C, several additional components with low intensity appear at higher binding energies (687.8 and 689.5 eV). These components could also be attributed to fluorine atoms in solid solution $TiO_{2-x}F_x$, but with higher O/F ratio in lattice. Therefore, the F 1s core peak evolution indicates that high TS temperatures promote the insertion/substitution of fluorine atoms in the atomic layers of oxide lattice.

The O 1s core peaks (Fig. 7) of single-phase $TiO_2$ anatase and rutile samples showed an asymmetric peak which can be decomposed into a main peak ($O_I$ at 530.1 eV) assigned to oxygen atoms of $TiO_2$ lattice and a minor peak ($O_{II}$ at 531.6 eV) assigned to surface OH groups [21]. When these oxides were fluorinated from 400 °C, we observed an additional weak component located at 532.9 eV ($O_{III}$). It could be attributed to water molecules adsorbed on the catalysts surface [22] or/and C—O bounds. The calculation of $O_{II}$/Ti atomic ratios (Table 4) indicated an increase of surface OH group content after the fluorination. The maximum $O_{II}$/Ti value reached a value of 0.38 for AFTO-600 and 0.48 for RFTO-600. This result highlights the creation of surface OH groups after surface fluorination by TS method, which was also observed on the fluorinated

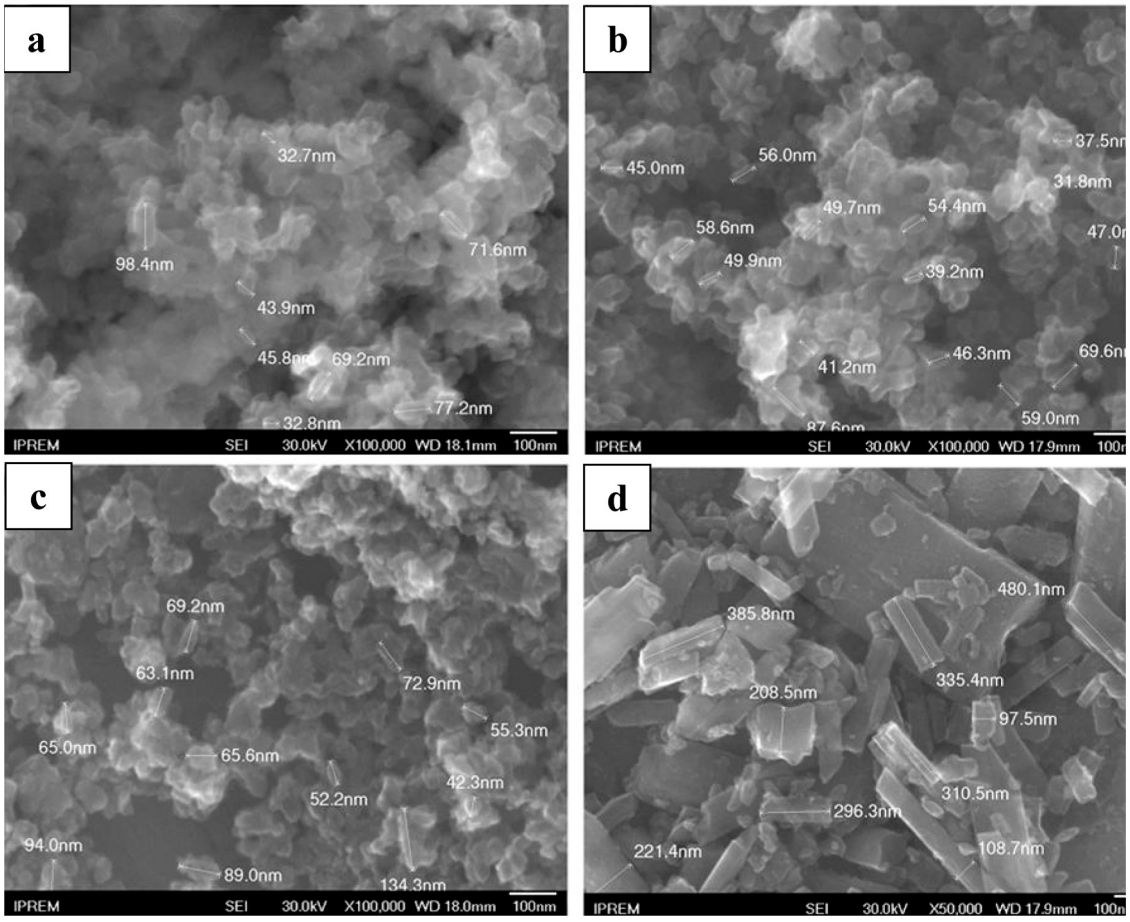


**Fig. 4.** SEM micrographs of (a) rutile, (b) RFTO-500, (c) RFTO-600 and (d) RFTO-950.

samples from $TiO_2$ P25 [9]. We can note that the increase of surface OH group content is larger for the fluorinated rutile $TiO_2$. Moreover, if we look after the $O_I$/Ti ratio value, we can identify two kinds of behaviour after the fluorination (Table 4). First, as the $O_I$/Ti ratios were lower than 2 for the fluorinated anatase $TiO_2$ from 400 to 600 °C, we suggest that the fluorination create oxygen vacancies on the surface. On the other hand, for the $TiO_2$ rutile fluorinated from 400 to 500 °C, the $O_I$/Ti ratios were superior to 2 which means that, the fluorination of rutile in this TS temperature range could lead the formation of titanium vacancies on the oxide surface.

## 4. Photocatalytic activity

### 4.1. Adsorption process

As the photocatalytic reactions occur on the surface of catalysts, the adsorption of organic compounds on its surface is a key element of the photocatalytic process. Fig. 8 shows a comparison of MB percentage adsorbed onto different samples at adsorption equilibrium. All fluorinated samples exhibit adsorption capacity of MB than the naked single-phase $TiO_2$ samples (12.3% for anatase and 10.4% for rutile). Moreover, the MB adsorption property globally increases with TS temperature for the samples fluorinated from 400 to 700 °C. The largest MB content on the catalysts surface was obtained for the AFTO-600 (67.5%) and RFTO-700 (82.8%) samples, which coincide with the highest $F_I$/Ti ratio obtained for these samples. However, above TS temperature of 700 °C, the MB adsorption property drastically decreases. Although the surface fluoride amount is the largest for the AFTO-950 and RFTO-950 catalysts, the adsorbed MB percentage is quite low with values of 21.6% and 25.9%, respectively.

The evolution of adsorbed MB content on these catalysts was found to be proportional to the chemisorbed $F^-$ amount observed by XPS analysis on their surface and inversely proportional to the particle size. Indeed, it is easy to understand that the adsorption of organic compounds on the surface of fluorinated $TiO_2$ depends greatly on the chemisorbed $F^-$ anions, the crystallite phase of catalyst and the particle size. For the fluorination at TS temperatures < 700 °C, the adsorption of MB on the $TiO_2$ surface is mainly affected by the electrostatic interactions between the organic molecules and the oxide surface since the phase composition and the particle size were not yet strongly modified. It was noticed in the literature that the amount of surface acid sites greatly is increasing after the fluorination of $TiO_2$ [5,23] which is explained by the presence of the strong electronegative fluoride anions on its surface. The fluoride anions tend to increase the positively charged of the neighbouring titanium atoms which can thus acting as Lewis acid sites. These sites could interact with the negatively charged $\pi$ electrons of the aromatic compounds [23], such as MB and therefore promote its adsorption. For the catalysts fluorinated at higher TS temperature (>700 °C), the formation and the growth of the$K_2Ti_6O_{13}$ particles, observed by SEM, lead to the decrease of the specific area of fluorinated samples. Therefore, the MB adsorption was fairly hindered for the samples fluorinated at 950 °C. An investigation of the surface reactivity in term of acidobasicity is engaged and will be published later.

### 4.2. UV light induced photocatalytic activity

The activity of these samples was tested by the photocatalytic MB degradation under UV light. Fig. 9 compares the

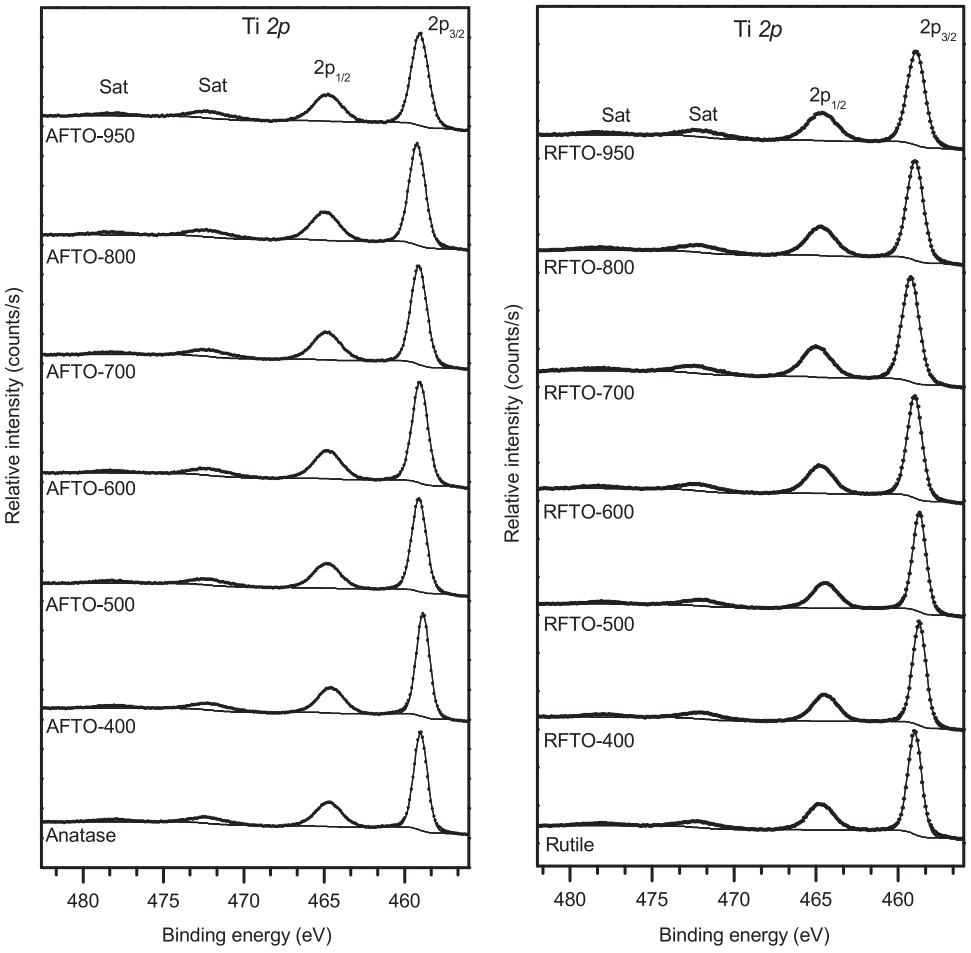


**Fig. 5.** Ti 2p spectra of fluorinated samples.

time-dependent profiles of MB degradation on the as-prepared photocatalysts from anatase/rutile under UV light irradiation. The rate constants were determined by plotting $\ln(C/C_0)$ versus time ($C$ is the MB concentration at time $t$ and $C_0$ is the initial MB concentration). It was found that the net decomposition of MB in the aqueous solution followed the pseudo-first-order Langmuir–Hinshelwood kinetic model. The rate constant ($k$) of MB degradation respectively reaches 0.31 $h^{-1}$ on the naked anatase $TiO_2$ and 0.36 $h^{-1}$ on the naked rutile $TiO_2$. The degradation rate was clearly enhanced by the surface fluorination of samples at 400 °C and 500 °C. The best photocatalytic activity was found in AFTO-500 catalyst with $k = 2.36\ h^{-1}$ (about seven times higher than pure anatase) and in RFTO-500 catalyst with $k = 0.94\ h^{-1}$ (about three times higher than pure rutile). The results also showed that the TS fluorination at 500 °C on $TiO_2$ anatase seems to be more efficient than $TiO_2$ rutile for photocatalytic applications. This observation is slightly different from literature. Xu et al. [24] reported that the surface fluorination can only increase the photocatalytic activity of $TiO_2$ anatase, but reduce the activity of $TiO_2$ rutile for the degradation of phenol under UV light irradiation. The reduced photocatalytic activity of $TiO_2$ rutile for the degradation of Brilliant Red X3B, an anionic azo dye by surface fluorination was also observed in the study of Lv et al. [25]. This shows that the thermal shock method used to fluorinate $TiO_2$ in our work plays an important role for the photocatalytic activity of fluorinated $TiO_2$, especially for the fluorinated $TiO_2$ rutile. However, the MB degradation rate began to decrease on the fluorinated samples prepared from 600 to 950 °C. The rate constant on AFTO-950 and RFTO-950 catalysts was respectively about five times and three times lower than that on AFTO-500 and RFTO-500 catalysts.

Compared to the results of characterization experiments, we observed that the photocatalytic activity of fluorinated $TiO_2$ anatase/rutile under UV irradiation was not only strongly affected by the phase composition, the particle size, but also the surface composition. At low TS temperatures, the phase composition of $TiO_2$ anatase/rutile was not modified, but the rate constant of MB degradation increased with the surface OH groups and the surface F atoms. At high TS temperature, although the chemisorbed and inserted fluorine content kept increasing, the activity declines dramatically with the formation of $K_2Ti_6O_{13}$ phase and the growth of particle size. Therefore the enhancement of the photocatalytic properties of fluorinated $TiO_2$ at TS temperatures below 600 °C finds its origin in the presence of $F^-$ ions on the surface and the increase of surface OH groups. It has been well known that the $OH^\bullet$ radicals act as oxidizing agents for organic compounds. For the naked $TiO_2$, according to the mechanism of $OH^\bullet$ radical formation under light illumination, most $OH^\bullet$ radicals are formed from the reaction of photo-generated hole ($h^+$) and surface hydroxyl groups (1), and remain adsorbed on $TiO_2$ surface [2,26]. When the oxide surface was fluorinated by TS method at 400 and 500 °C, the surface hydroxyl group content strongly increased (Table 4) which would enhance the content of $OH^\bullet$ radicals on the surface and thus improve the photocatalytic activity.

$$\equiv\text{Ti-OH} + h_{vb}{}^{+} \rightarrow \equiv\text{Ti-OH}^{\bullet+} \quad (1)$$

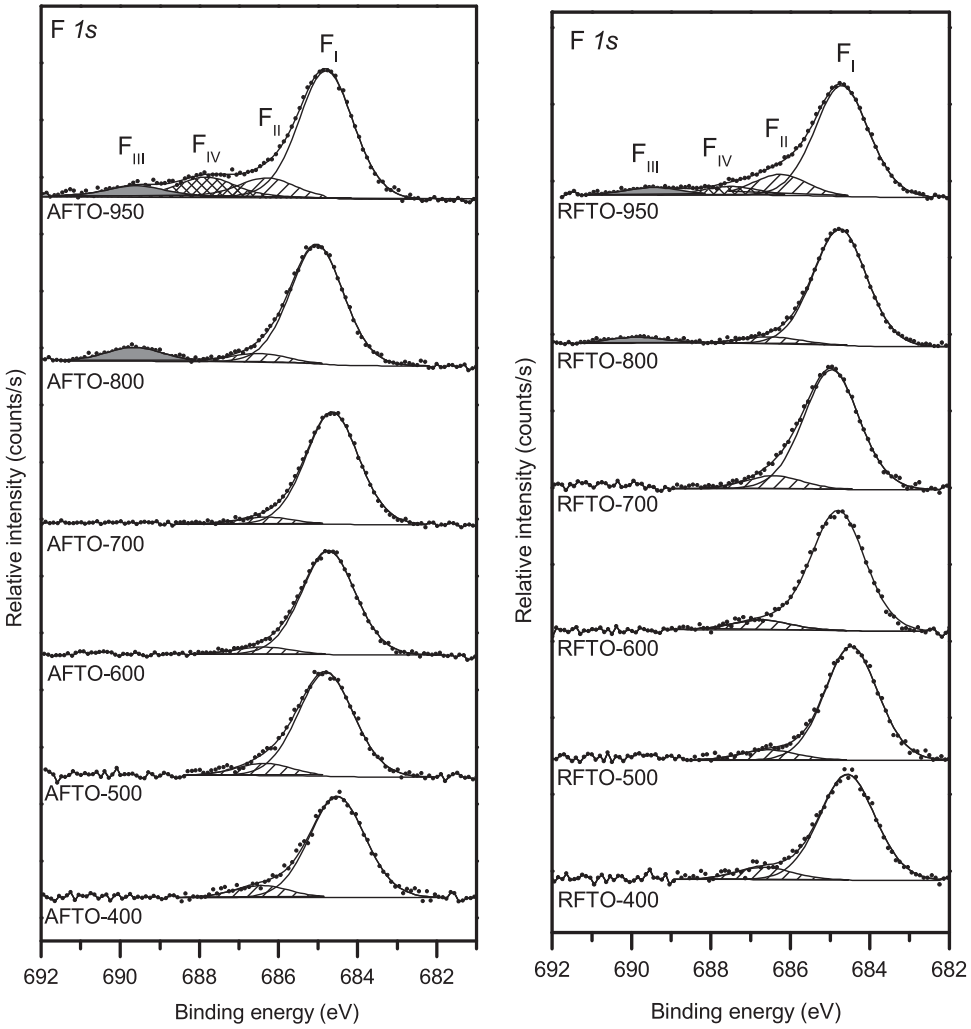


**Fig. 6.** F 1s spectra of all fluorinated samples from anatase (a) and rutile (b) $TiO_2$.

On the other hand, the formation of surface fluoride species also enhances the hole availability of $TiO_2$ [6,27]. More available photogenerated holes induce the fact that they are not only trapped at the site of surface OH groups, but also accessible for reaction with water in order to create mobile free $OH^{\bullet}$ radicals in solution (2) [26]. These mobile free radicals can quickly react with MB molecules in solution and therefore improve the photocatalytic activity of $TiO_2$.

$$\equiv\text{Ti-F} + H_2O(\text{or}OH^-) + h_{vb}{}^+ \rightarrow \equiv\text{Ti-F} + OH^{\bullet}{}_{free} + H^+ \quad (2)$$

These results highlighted the advantages of our fluorination process by TS method: a simple, low cost method which is only performed at low temperature and for a short time can remarkably improve the UV light responses of $TiO_2$. The results also showed that the fluorinated catalysts from anatase always present the higher photocatalytic activity than that from rutile under UV irradiation. This indicated the different effects of fluorination by TS method on the photocatalytic activity of $TiO_2$, depending on its crystal structure.

For the catalysts fluorinated at TS temperatures above 600 °C, the reduction of UV induced photocatalytic activity should be explained by the formation of $K_2Ti_6O_{13}$ phase. The photocatalytic performance of $M_2Ti_6O_{13}$ (M = Na, K) titanate phases for the degradation of water pollutants has been also studied [28–32]. Under UV irradiation, $K_2Ti_6O_{13}$ showed a good photocatalytic performance for the degradation of acetic acid [29] while $Na_2Ti_6O_{13}$ can decompose the 4-chlorophenol ($k = 0.48\ min^{-1}$) [30] and MB ($k = 0.01\ min^{-1}$) [32]. Nevertheless, the comparison of photocatalytic activity between $K_2Ti_6O_{13}$ and $TiO_2$ is so far not clear. $K_2Ti_6O_{13}$ prepared by solid-state reaction of stoichiometric mixture of potassium carbonate and titania at 900 °C for 24 h presents a lower activity than Evonik Aeroxide $TiO_2$ P25 [29]. Conversely, a mixture of $K_2Ti_6O_{13}$ and anatase, prepared by a hydrothermal reaction of $TiO_2$ P25 with potassium hydroxide at 110 °C for 20 h followed by calcination at 700 °C for 1 h, has a superior photocatalytic activity to that of $TiO_2$ P25 in the degradation of acetic acid [29]. In our study, the rate constant of MB degradation decreased with the formation of $K_2Ti_6O_{13}$ phase, indicating that the $K_2Ti_6O_{13}$ formation seems to be one of factors which hinder the photocatalytic degradation of MB. On the other hand, the high TS temperatures induce the particle growth which makes decrease the specific surface area. It has been well known that the specific surface area plays an important role in efficiency of heterogeneous photocatalyst [33,34]. This decrease could affect the amount of surface OH group and then reduce the photocatalytic activity. Furthermore, a lower specific surface area also limits the diffusion of photoexcited electron–hole pairs on the surface. In consequence, the surface recombination of electron–hole pairs is promoted, which suppresses the quantum efficiency of MB photocatalytic degradation.

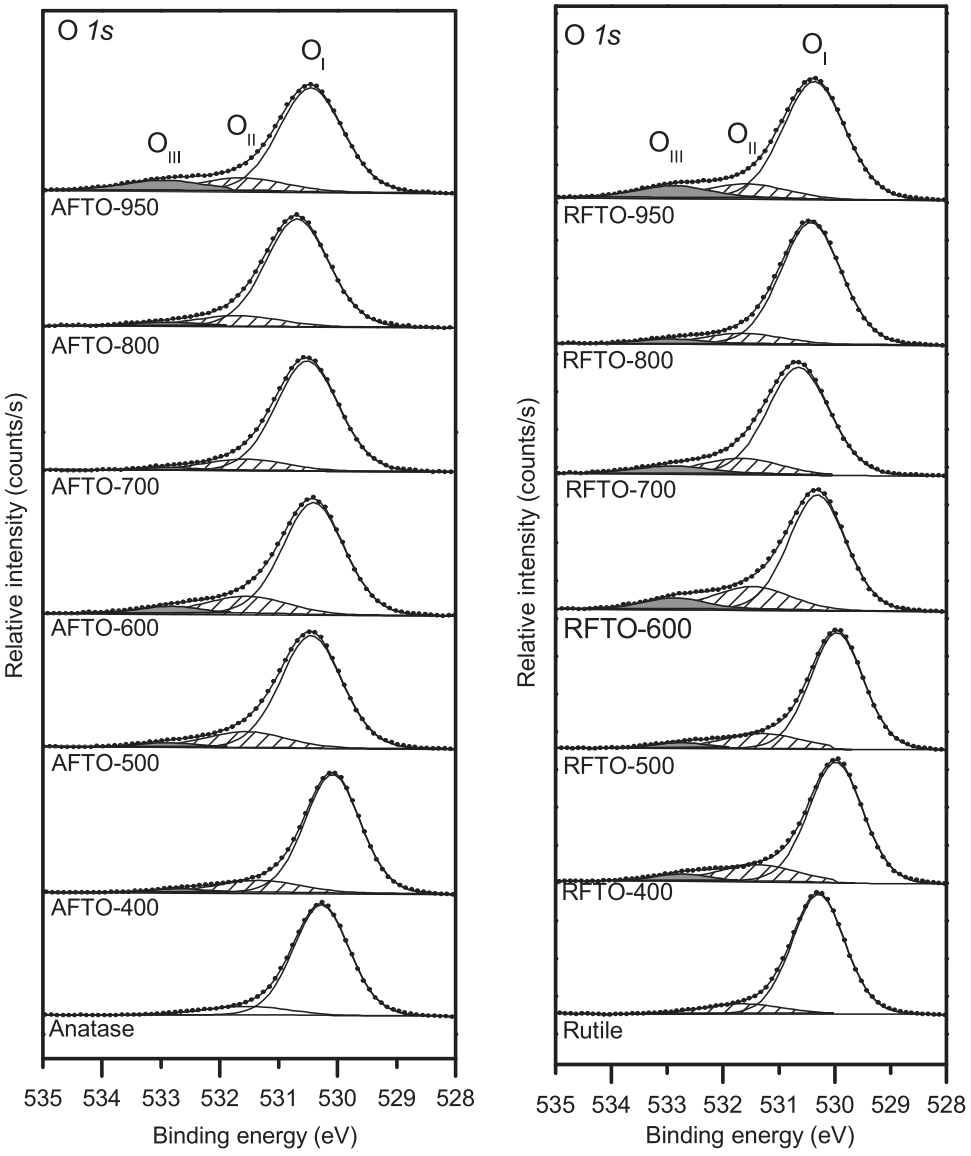


**Fig. 7.** O 1s spectra of naked $TiO_2$ and all fluorinated samples from anatase (a) and rutile (b) $TiO_2$.

### 4.3. Visible light induced photocatalytic activity

Visible light induced photocatalytic activity of fluorinated catalysts was also evaluated via the MB degradation. The time-dependent profiles of MB degradation on naked and fluorinated samples from anatase/rutile under visible light irradiation were compared in Fig. 10. The naked $TiO_2$ anatase almost did not operate under visible light ($k = 0.03\ h^{-1}$) whereas the naked $TiO_2$ rutile presented a good photocatalytic activity ($k = 0.26\ h^{-1}$). This is not surprising since the $TiO_2$ anatase possesses a bandgap (3.2 eV) [35]

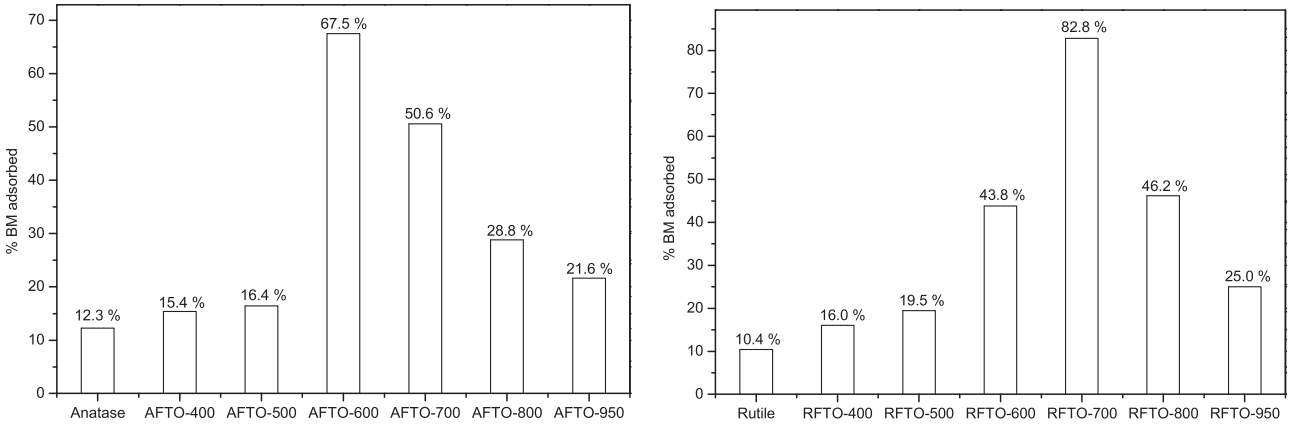


**Fig. 8.** Comparison of MB amount adsorbed on the surface of fluorinated samples from anatase (a) and rutile (b).

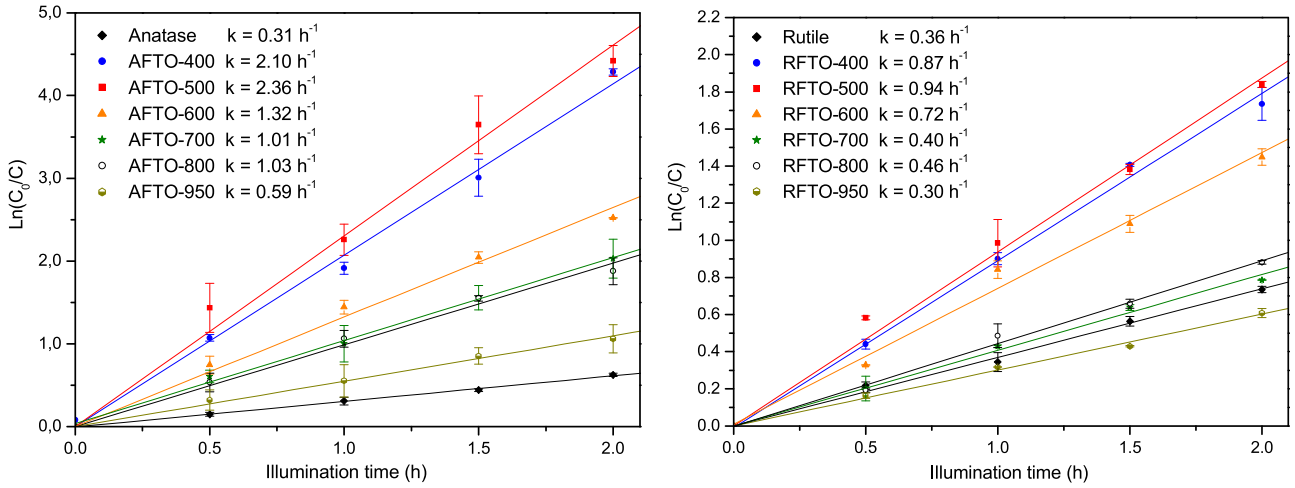


**Fig. 9.** Ln($C_0/C$) versus time plot of MB degradation under UV irradiation on fluorinated samples from anatase (a) and from rutile (b). $C$ is the MB concentration (mol $L^{-1}$) at time $t$ and $C_0$ is the initial MB concentration (mol $L^{-1}$).

wider than $TiO_2$ rutile (3.0 eV) [36] and thus the energy of visible light (420 nm) was not enough to excite $TiO_2$ anatase.

We also observed the similar evolution of photocatalytic activity of samples under visible light irradiation (420 nm) in comparison to that under UV light irradiation (350 nm). All the AFTO and RFTO samples prepared from 400 to 600 °C presented higher photocatalytic degradation rate of MB than that of their naked $TiO_2$ samples. The AFTO-600 and RFTO-500 samples showed the best photocatalytic activity, with $k = 0.26\ h^{-1}$ (about eight times higher than $TiO_2$ pure anatase) and $0.40\ h^{-1}$ (about two times higher than $TiO_2$ pure rutile), respectively. More especially, the RFTO-500 catalyst exhibits a rate constant of MB degradation larger than the best photocatalyst based on fluorinated $TiO_2$ P25 at 500 °C ($k = 0.32\ h^{-1}$) reported in our previous study [9]. For the oxides fluorinated in the 700–950 °C temperature range, their photocatalytic activity decreased with the TS temperatures.

These results show that the surface fluorination by TS method at temperatures below 700 °C can effectively increase the activity of $TiO_2$ under visible light irradiation. It was surprising since most studies in F-doping reported that F atoms inserted in the bulk or adsorbed on the surface can not modify the optical properties of $TiO_2$, neither in band gap narrowing nor in creation of new absorption band for the activity under visible light illumination. The visible light induced photocatalytic performance of these samples should be explained by other factors. In our previous work [9], we observed the surface substoechiometry for the fluorinated oxides prepared from 400 to 600 °C, meaning that the TS method can produce the oxygen vacancies on the oxides surface. In this study, we also observed the formation of oxygen vacancies on the surface of AFTO-400, AFTO-500 and AFTO-600. These oxygen vacancies could create two types of shallow trap in the electronic structure of $TiO_2$: F centre with two trapped electrons and $F^+$ centre with one trapped electron. Their electronic state is respectively located at 0.5 and 0.8 eV below the conduction band [5,37,38]. Then the photocatalytic processes can occur via the photoexcitation of extrinsic absorption bands originated from F and $F^+$ centres which requires less energy. These arguments allow us to explain the origin of the enhanced photocatalytic performances of $TiO_2$ samples fluorinated at 400–600 °C from anatase under visible light illumination. On the other hand, XRD patterns indicated the formation of rutile phase in the AFTO-600 sample, which could also promote the photocatalysis under visible light. Thus the formation of oxygen vacancies and rutile phase in this sample made it become the best photocatalyst among the fluorinated samples from $TiO_2$ anatase.

However, for $TiO_2$ fluorinated from rutile at 400 and 500 °C, we did not observe the presence of oxygen vacancies, but the

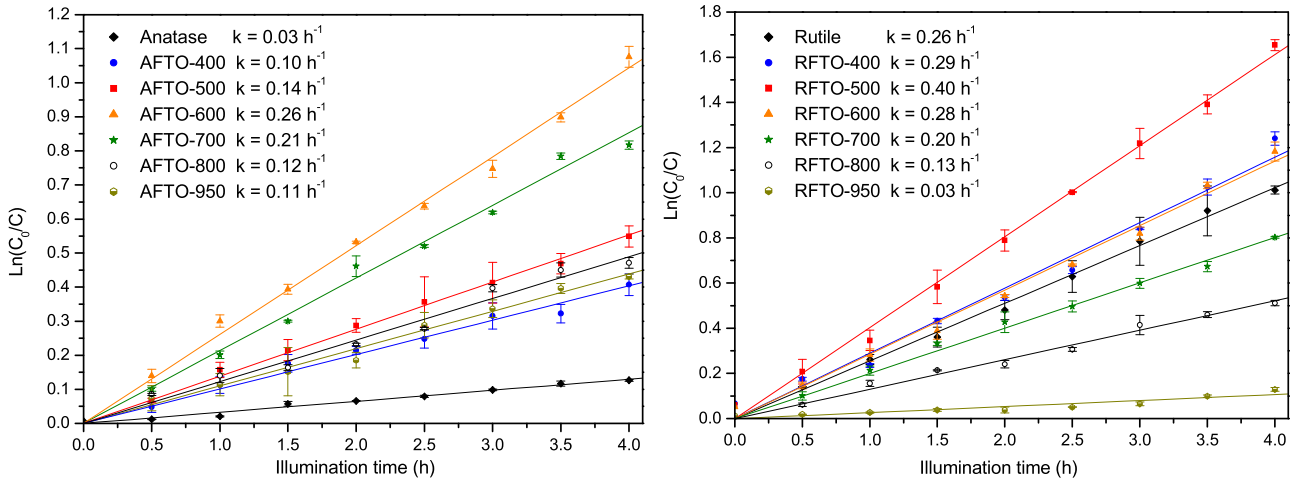


**Fig. 10.** Ln($C_0/C$) versus time plot of MB degradation under visible light irradiation on fluorinated samples from anatase (a) and from rutile (b). $C$ is the MB concentration (mol $L^{-1}$) at time $t$ and $C_0$ is the initial MB concentration (mol $L^{-1}$).

**Table 3**
High resolution XPS data of fluorinated rutile $TiO_2$ samples: binding energies (eV), FWHM (eV) in parentheses and atomic percentages (%).

| | Rutile | | RFTO-400 | | RFTO-500 | | RFTO-600 | | RFTO-700 | | RFTO-800 | | RFTO-950 | |
|---|---|---|---|---|---|---|---|---|---|---|---|---|---|---|
| | $E_B$ (FWHM) eV | % | $E_B$ (eV) | % | $E_B$ (eV) | % | $E_B$ (eV) | % | $E_B$ (eV) | % | $E_B$ (eV) | % | $E_B$ (eV) | % |
| C 1s | 285.0 (1.5) | 11.1 | 285 (1.4) | 7.1 | 285.0 (1.4) | 7.1 | 285.0 (1.5) | 7.9 | 285.0 (1.5) | 9.9 | 285.0 (1.4) | 8.4 | 285.0 (1.4) | 8.5 |
| | 286.7 (1.2) | 1.4 | 286.4 (1.5) | 0.9 | 286.5 (1.1) | 0.6 | 286.5 (1.5) | 0.9 | 286.1 (1.6) | 1.5 | 286.3 (1.6) | 0.9 | 286.4 (1.5) | 1.0 |
| | 289.0 (1.5) | 1.2 | 289.1 (1.5) | 0.5 | 289.3 (1.4) | 0.3 | 289.3 (1.2) | 0.4 | 289.7 (1.2) | 0.6 | | | | |
| Ti $2p_{3/2-1/2}$ | 459.0–464.7 (1.0–1.9) | 26.4 | 458.7–464.5 (1.0–1.8) | 23.5 | 458.7–464.5 (1.0–1.8) | 23.6 | 459.0–464.8 (1.1–1.9) | 23.0 | 459.2–465.0 (1.3–2.1) | 23.5 | 459.0–464.7 (1.2–2.0) | 22.5 | 458.9–464.6 (1.3–2.1) | 20.7 |
| Satellites | 471.8–478.1 | | 471.7–478.1 | | 471.8–477.9 | | 471.8–478.2 | | 471.9–478.3 | | 471.9–478.2 | | 471.5–478.1 | |
| O1s I | 530.3 (1.1) | 53.3 | 530.0 (1.1) | 49.6 | 530.0 (1.1) | 51.6 | 530.3 (1.2) | 45.7 | 530.6 (1.3) | 46.6 | 530.4 (1.3) | 45.2 | 530.4 (1.3) | 41.7 |
| O1s II | 531.6 (1.6) | 6.7 | 531.4 (1.6) | 9.4 | 531.5 (1.6) | 9.0 | 531.6 (1.6) | 11.0 | 531.6 (1.6) | 7.3 | 531.6 (1.6) | 4.8 | 531.6 (1.6) | 5.8 |
| O1s III | | | 532.7 (1.6) | 3.7 | 532.9 (1.6) | 1.8 | 532.9 (1.6) | 4.6 | 532.9 (1.6) | 2.8 | 532.9 (1.6) | 2.2 | 532.8 (1.5) | 5.0 |
| F1s I | | | 684.6 (1.6) | 2.4 | 684.5 (1.6) | 2.6 | 684.8 (1.6) | 3.2 | 685.0 (1.6) | 4.1 | 684.8 (1.6) | 6.4 | 684.7 (1.6) | 6.5 |
| F1s II | | | 686.7 (1.6) | 0.3 | 686.5 (1.6) | 0.3 | 686.7 (1.6) | 0.4 | 686.4 (1.65) | 0.3 | 686.5 – 689.8 (1.65) | 0.8 | 686.6 – 689.2 (1.6) | 1.9 |
| K2$p_{3/2-1/2}$ I | | | 292.7–295.5 (1.1–1.2) | 1.3 | 292.8–295.6 (1.2–1.3) | 1.5 | 292.9–295.7 (1.4–1.4) | 1.2 | 292.9–295.6 (1.0–1.2) | 1.8 | 292.7–295.5 (1.1–1.1) | 6.3 | 292.6–295.4 (1.1–1.1) | 6.1 |
| K2$p_{3/2-1/2}$ II | | | 293.6–296.3 (1.2–1.2) | 1.2 | 293.6–296.3 (1.2–1.3) | 1.3 | 293.7–296.3 (1.4–1.4) | 1.6 | 293.6–296.3 (1.1–1.3) | 1.5 | 293.6–296.3 (1.1–1.2) | 2.5 | 293.7–296.4 (1.2–1.3) | 2.7 |

**Table 4**
Comparison of $O_{lattice}$/Ti ($O_I$/Ti), $O_{OH}$/Ti ($O_{II}$/Ti), $F_{chemisorbed}$/Ti ($F_I$/Ti) and $F_{inserted}$/Ti ($F_{II}$/Ti) ratios of naked $TiO_2$ anatase and rutile and fluorinated samples from XPS data.

| | TS temperature (C) | | | | | | |
|---|---|---|---|---|---|---|---|
| | Naked sample | 400 | 500 | 600 | 700 | 800 | 950 |
| $O_I$/Ti | AFTO | 2 | 1.94 | 1.94 | 1.94 | 1.98 | 1.99 | 1.99 |
| | RFTO | 2.02 | 2.1 | 2.16 | 1.98 | 1.98 | 2 | 2.01 |
| $O_{II}$/Ti | AFTO | 0.23 | 0.28 | 0.28 | 0.38 | 0.29 | 0.24 | 0.29 |
| | RFTO | 0.26 | 0.4 | 0.38 | 0.48 | 0.31 | 0.21 | 0.28 |
| $F_I$/Ti | AFTO | | 0.09 | 0.13 | 0.2 | 0.25 | 0.17 | 0.22 |
| | RFTO | | 0.1 | 0.12 | 0.14 | 0.18 | 0.28 | 0.31 |
| $F_{II}$/Ti | AFTO | | 0.01 | 0.01 | 0.02 | 0.02 | 0.03 | 0.08 |
| | RFTO | | 0.01 | 0.01 | 0.02 | 0.02 | 0.04 | 0.09 |

formation of titanium vacancies. Interestingly, it was reported that the titanium vacancies can also create the acceptor states located at 0.88 eV above the valence band [39] and then reduce the required energy for the photoexcitation. As a result, the RFTO-400 and RFTO-500 showed the highest rate constants for MB degradation under visible light illumination. The photocatalytic activity under visible light of RFTO-500 catalyst was higher than AFTO-600 one and the best fluorinated photocatalyst based on $TiO_2$ P25 ($k = 0.31\ h^{-1}$ [9]). Therefore the results highlighted the important role of $TiO_2$ starting phase in the effects of fluorination on its photocatalytic activity.

Above TS temperature of 700 °C, the visible light induced photocatalytic activity decreased. This phenomenon can be also explained by the decrease of oxygen vacancies, titanium vacancies and more especially by the $K_2Ti_6O_{13}$ formation. Wang et al. [40] investigated the UV-Visible absorption spectrum of $K_2Ti_6O_{13}$ nanowires and found the maximum absorption edge at 365 nm, corresponding to a band gap value of 3.40 eV, meaning that the photocatalysis on $K_2Ti_6O_{13}$ cannot operate under visible light. Thus, the formation of this structure in our catalysts definitely decreases their activity for MB degradation.

## 5. Conclusion

Fluorinated catalysts from anatase and rutile monophasic $TiO_2$ were prepared using the thermal shock method for the large temperature range from 400 to 950 °C. For the TS temperature range of 400–500 °C, the fluorination did not modify neither the crystal structure, nor the morphology of $TiO_2$ anatase/rutile but successfully created fluoride ions chemisorbed on the surface and fluorine atoms inserted in $TiO_2$ lattice. XPS analyses also indicated the increase of surface OH groups and the formation of oxygen vacancies for $TiO_2$ anatase and titanium vacancies for $TiO_2$ rutile due to the surface fluorination. These modifications did not only improve the photocatalytic activity under UV irradiation but also under visible light illumination. The best rate constants of MB degradation were observed for AFTO-500 ($k = 2.36\ h^{-1}$) under UV and RFTO-500 ($k = 0.40\ h^{-1}$) under visible light irradiation. The results demonstrated that the fluorination by thermal shock method is a simple and efficient way to improve the photocatalytic behaviour of $TiO_2$. Above 600 °C, for both $TiO_2$ anatase and $TiO_2$ rutile, the fluorination leads the formation of $K_2Ti_6O_{13}$ and the increase of particle size, which decrease their photocatalytic activity.

## Acknowledgment

This research is funded by Vietnam National Foundation for Science and Technology Development (NAFOSTED) under grant number 104.02-2012.53.

## References


[1] A. Fujishima, T.N. Rao, D.A. Tryk, J. Photochem. Photobiol. C 1 (2000) 1.
[2] C. Minero, G. Mariella, V. Maurino, E. Pelizzetti, Langmuir 16 (2000) 8964.
[3] J.S. Park, W. Choi, Langmuir 20 (2004) 11523.
[4] J.C. Yu, J. Yu, W. Ho, Z. Jiang, L. Zhang, Chem. Mater. 14 (2002) 3808.
[5] D. Li, H. Haneda, S. Hishita, N. Ohashi, N.K. Labhsetwar, J. Fluorine Chem. 126 (2005) 69.
[6] S.Y. Yang, Y.Y. Chen, J.G. Zheng, Y.J. Cui, J. Environ. Sci. 19 (2007) 86.
[7] Y. Chen, F. Chen, J. Zhang, Appl. Surf. Sci. 255 (2009) 6290.
[8] L. Junqi, W. Defang, L. Hui, H. Zuoli, Z. Zhenfeng, Appl. Surf. Sci. 257 (2011) 5879.
[9] T.K. Le, D. Flahaut, D. Foix, S. Blanc, H.K.H. Nguyen, T.K.X. Huynh, H. Martinez, J. Solid State Chem. 187 (2012) 300.
[10] R.I. Bickley, T. Gonzalez-Carreno, J.S. Lees, L. Palmisano, R.J.D. Tilley, J. Solid State Chem. 92 (2001) 178.
[11] B. Zielinska, J. Grzechulska, B. Grzmil, A.W. Morawski, Appl. Catal. B 35 (2001) L1.
[12] A. Rachel, M. Sarakha, M. Subrahmanyam, P. Boule, Appl. Catal. B 37 (2002) 293.
[13] K. Komaguchi, H. Nakano, A. Araki, Y. Harima, Chem. Phys. Lett. 428 (2003) 338.
[14] D.A. Shirley, Phys. Rev. B 5 (1972) 4709.
[15] J.H. Scofield, J. Electron Spectrosc. Relat. Phenom. 8 (1976) 129.
[16] J. Rodriguez-Carvajal, IUCr Newslett. 26 (2001) 12.
[17] R.G. Nair, S. Paul, S.K. Samdarshi, Sol. Energ. Mater. Sol. Cells 95 (2011) 1901.
[18] M.G. Faba, D. Gonbeau, G. Pfister-Guillouzo, J. Electron. Spectrosc. Relat. Phenom. 73 (1995) 65.
[19] M.C. Biesinger, L.W.M. Lau, A. Gerson, R.St.C. Smart, Appl. Surf. Sci. 257 (2010) 887.
[20] Y. Xie, X. Zhao, Y. Li, Q. Zhao, X. Zhou, Q. Yuan, J. Solid State Chem. 181 (2008) 1936.
[21] J.C. Dupin, D. Gonbeau, P. Vinatier, A. Levasseur, Phys. Chem. Chem. Phys. 2 (2000) 1319.
[22] H. Jiang, H. Song, Z. Zhou, X. Liu, G. Meng, J. Phys. Chem. Solids 68 (2007) 1830.
[23] D.G. Huang, S.-J. Liao, J.-M. Liu, Z. Dang, L. Petrik, J. Photochem. Photobiol. A 184 (2006) 282.
[24] Y. Xu, K. Lv, Z. Xiong, W. Leng, W. Du, D. Liu, X. Xue, J. Phys. Chem. C 111 (2007) 19024.
[25] K. Lv, X. Li, K. Deng, J. Sun, X. Li, M. Li, Appl. Catal. B: Environ. 95 (2010) 383.
[26] C. Minero, G. Mariella, V. Maurino, E. Pelizzetti, Langmuir 16 (2000) 2632.
[27] C. Yu, M. J.C.Yu, J. Chan, Solid State Chem. 182 (2009) 1061.
[28] R.B. Yahya, H. Hayashi, T. Nagase, T. Ebina, Y. Onodera, N. Saitoh, Chem. Mater. 13 (2001) 842.
[29] F. Amano, T. Yasumoto, T. Shibayama, S. Uchida, B. Ohtani, Appl. Catal. B: Environ. 89 (2009) 583.
[30] V. Štengl, S. Bakardjieva, J. Šubrt, E. Večerníková, L. Szatmary, M. Klementová, V. Balek, Appl. Catal. B: Environ. 63 (2006) 20.
[31] L. Zhen, C.Y. Xu, W.S. Wang, C.S. Lao, Q. Kuang, Appl. Surf. Sci. 255 (2009) 4149.
[32] L.M. Torres-Martínez, I. Juárez-Ramírez, K.D. Ángel-Sánchez, L. Garza-Tovar, A. Cruz-López, G.D. Ángel, J. Sol–Gel Sci. Technol. 47 (2008) 158.
[33] J. Yu, W. Wang, B. Cheng, B.-L. Su, J. Phys. Chem. C 113 (2009) 6743.
[34] N. Arconada, A. Durán, S. Suárez, R. Portela, J.M. Coronado, B. Sánchez, Y. Castro, Appl. Catal. B 86 (2009) 1.
[35] A. Welte, C. Waldauf, C. Brabec, P. Wellmann, Thin Solid Films 516 (2008) 7256.
[36] J. Pascual, J. Camassel, H. Mathieu, Phys. Rev. Lett. 39 (1977) 1490.
[37] D. Li, H. Haneda, N.K. Labhsetwar, S. Hishita, N. Ohashi, Chem. Phys. Lett. 401 (2005) 579.
[38] W. Ho, J.C. Yu, S. Lee, Chem. Commun. 10 (2006) 1115.
[39] Z. Zhou, M. Li, L. Guo, J. Phys. Chem. Solids 71 (2010) 1707.
[40] B.L. Wang, Q. Chen, R.H. Wang, L.-M. Peng, Chem. Phys. Lett. 376 (2003) 726.